Construction and Building Materials 489 (2025) 142348

Contents lists available at ScienceDirect

Construction and Building Materials

journal homepage: www.elsevier.com/locate/conbuildmat

Experimental characterisation of the friction coefficient of mortar bed joints in clay-brick masonry

Lewis J. Gooch [a,b,*,1], Mark J. Masia [a,2], Mark G. Stewart [b,3], Michele Spadari [c]

[a] Critical Infrastructure Performance and Reliability Research Group, The University of Newcastle, Callaghan, NSW 2308, Australia
[b] Centre for Built Infrastructure Resilience, University of Technology Sydney, Ultimo, NSW 2007, Australia
[c] College of Engineering, Science and Environment, The University of Newcastle, Callaghan, NSW 2308, Australia

ARTICLE INFO

Keywords:
Clay-brick masonry
Shear strength
Friction
Structural reliability
Probability

ABSTRACT

Understanding the characteristics of material properties is an important aspect of the design of new, and assessment of existing, structures. Furthermore, the development of accurate statistical models of these properties is critical to a reliability-based assessment of structures. Examining the properties of masonry materials has been the subject of many publications, but few consider the friction behaviour of the brick-mortar interface under shear loading. This paper presents an extensive repetitive laboratory testing study where the residual friction responses of a range of extruded (perforated), pressed (frogged) and solid clay bricks have been observed under direct shear loading at various levels of pre-compressive normal stress. The sensitivity of this friction resistance to the interlocking mechanisms of extruded and pressed brick masonry, as well as the amount of normal stress, has been considered, facilitating the determination of a suitable probabilistic model of the friction coefficient. It was determined that the residual friction coefficient of clay-brick masonry can be accurately approximated with a Normal (Gaussian) distribution, and is comparably variable to the masonry compression strength, with a coefficient of variation equal to 0.14. Furthermore, the influence that pre-existing, tension-induced cracking has on the friction coefficient has been examined. It was found that tension-induced cracks do not significantly affect the residual friction coefficient.

1. Introduction

The friction resistance of a mortar joint is a critical parameter that is considered in the design and assessment of masonry structures, particularly those subject to in-plane lateral loads. This property is prominent in the predictive models for in-plane shear behaviour presented by Turnšek and Čačovič [1], Magenes and Calvi [2], and most masonry design standards; NTC [3], AS 3700 [4], EN 1996–1-1 [5], TMS 402/602–22 [6] and CSA S304–24 [7]. Typically, a deterministic value of the friction coefficient (or shear friction factor), μ_f, is adopted, ranging in magnitude from 0.25 to 1.20 [8-10], and is determined from a test method such as the triplet test specified in EN 1052-3 [11]. However, despite the significance of this property to the behaviour of unreinforced masonry (URM) structures subject to shear loading and the large range of values that are evident in the literature, few studies investigate, or even consider, the statistical properties of the friction coefficient of mortar joints.

One such study by Gonen et al. [12] presents a series of numerical models that consider a variable angle of shearing, ϕ' (equal to arctan (μ_f)), in both spatial and non-spatial stochastic finite element analyses; adopting a mean angle of shearing equal to 35° ($\mu_f = 0.70$). The sensitivity of the peak in-plane shear resistance of stone masonry wall panels to the variability of ϕ' was assessed by adopting coefficients of variation (COVs) ranging from 0.05 to 0.25, and correlation coefficients for adjacent mortar joints of 0 (no correlation), 0.65, 0.85 and 1.0 (fully correlated). The results of this study indicate that a randomly variable friction coefficient can affect the peak load resistance by up to 10 %. However, a limitation of this investigation is that not all numerical

* Correspondence to: The University of Newcastle, University Drive, Callaghan NSW 2308 Australia.
E-mail addresses: lewis.gooch@newcastle.edu.au (L.J. Gooch), mark.masia@newcastle.edu.au (M.J. Masia), mark.stewart@uts.edu.au (M.G. Stewart), michele.spadari@newcastle.edu.au (M. Spadari).
[1] ORCID: 0000-0001-6764-3121
[2] ORCID: 0000-0002-1991-9602
[3] ORCID: 0000-0001-6887-6533

https://doi.org/10.1016/j.conbuildmat.2025.142348
Received 7 April 2025; Received in revised form 27 May 2025; Accepted 17 June 2025
Available online 24 June 2025

simulations produced a shear-sliding failure in the modelled walls (particularly for the non-correlated friction coefficients), limiting the influence of ϕ' on the peak load resistance. Furthermore, the adopted mean of $\phi' = 35°$ and the nominal COVs of 0.05, 0.15 and 0.25 have not been based on experimental testing. Thus, an accurate understanding of true variability of the friction coefficient is highly relevant to applications such as stochastic finite element modelling and structural reliability analyses.

The significance of accurately capturing the random variations in the friction coefficient of mortar joints in masonry walls is compounded by the fact that these interfaces are susceptible to cracking throughout their life due to a variety of factors such as mortar shrinkage, ground movement, and unfavourable loading conditions, such as those that induce tensile stresses. Due to the prevalence of existing cracking in masonry structures, the frictional resistance of the mortar joints is often the most significant component of resistance for URM walls subject to in-plane lateral loads. In addition, the frictional resistance of a mortar joint depends upon the mechanism by which the joint first cracks. It is noted by Magenes and Calvi [2] that the friction coefficient estimated from the residual shear sliding resistance is significantly lower than that for joints that are first cracked in tension before undergoing a sliding failure, as is common in URM shear walls subject to cyclic loads. This difference in the effective friction coefficient may be attributable to the formation of a shear failure surface that retains the additional resistance provided from mortar plugs for extruded bricks or a frog for pressed bricks, or due to a partially pre-defined sliding plane that has not yet been subject to surface roughness degradation.

The current study examines the friction behaviour of clay-brick masonry, including both the statistics of the friction coefficient of mortar joints between extruded (perforated), pressed (frogged) and solid bricks, as well as the influence that existing tension cracking has on the frictional resistance of a mortar joint. This investigation has been achieved through the application of extensive laboratory testing on replicate samples of clay-brick masonry couplets, constructed using a standardised [4] general purpose mortar mix.

2. Methodology

2.1. Masonry specimens

In this study, three types of extruded units, two types of pressed units, and one type of solid (no perforations or frog) unit were utilised, with a 1:1:6 (cement: lime: sand, by volume) mortar mix (approximately 1:0.5:7.6 by mass), as per AS 3700 [4], with water-cement ratios (by mass) ranging from 1.5 to 2.0. As the interlocking of masonry units is highly significant to the shear-sliding resistance of masonry, the perforation patterns of the extruded units and frog geometries of the pressed units are presented in Fig. 1; note that the extruded bricks Type E1 and E2 were used in both the pilot and final studies, while the remaining types were used only in the final study (refer to Sections 2.2 and 2.3). Additionally, all bricks maintained the standard Australian overall dimensions of 230 mm × 110 mm × 76 mm (length × thickness × height).

The use of six distinct brick types allowed for the influence that the different interlocking mechanisms had on the shear behaviour to be considered. In general, however, it was observed in testing that shear failures generally developed within the mortar joint, limiting the influence of mortar intruding within the bricks. As discussed in subsequent sections, the different brick types still exhibited distinct behaviours under direct shear loading. This is likely attributable to differing normal and shear stress distributions resulting from the stiffness of the brick material and influence of perforations/frogs.

2.2. Pilot study test set-up

The pilot study performed for this investigation considered only the shear behaviour of masonry specimens first cracked under direct tensile loading (see Section 4). These specimens were subject to shear loading via a bespoke testing apparatus that was developed considering the findings of Stöckl et al. [13] and the shear-couplet test developed by Van Der Pluijm [14]. This apparatus was fabricated such that shear forces were applied concentrically with the single mortar joint of the masonry couplet (see Fig. 2(a) and (c)).

Pre-cracking of the unit-mortar interfaces was initiated via direct tensile loading using the testing apparatus shown in Fig. 2(b) and (d). This initial tensile failure was induced in a subset of specimens to investigate the influence of pre-existing cracks on the shear behaviour masonry. It may be expected that a tension induced failure surface would be rougher (i.e.: maintain a higher friction coefficient) than the residual failure surface of masonry subject only to direct shear, as the grinding between shear planes may act to smooth the formed failure surface. To minimise any disturbance to the tensile failure surface, both the tensile- and shear-testing apparatuses were developed to be easily removable from the couplet specimens.

Some key limitations became evident during the application of both the pilot shear- and tension-testing methods. Foremost among these were issues related to the use of epoxy to adhere the steel plates to each specimen. Despite the use of a high-strength epoxy, the interface between the steel plates and masonry units was prone to failure during both the shear and tension tests prior to the intended shear- or tension-failures of the unit-mortar interface. Furthermore, the need to cure the

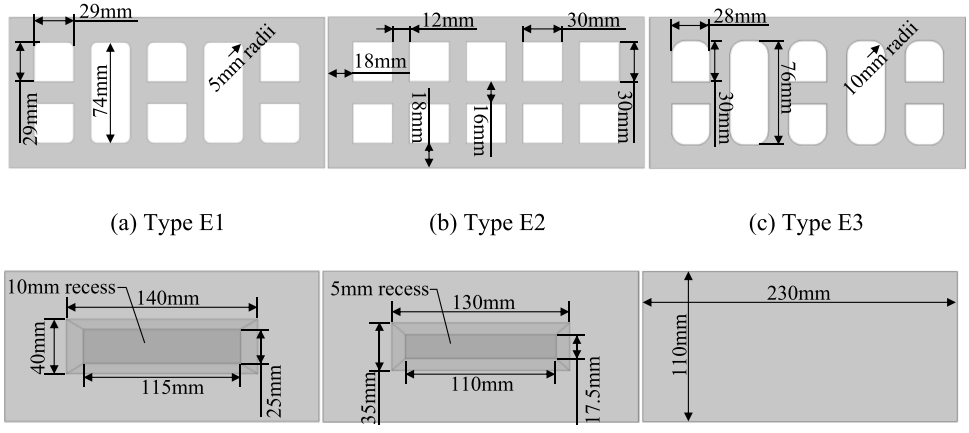

(a) Type E1 (b) Type E2 (c) Type E3

(d) Type P1 (d) Type P2 (e) Type S1

Fig. 1. Masonry unit geometries and perforation patterns.

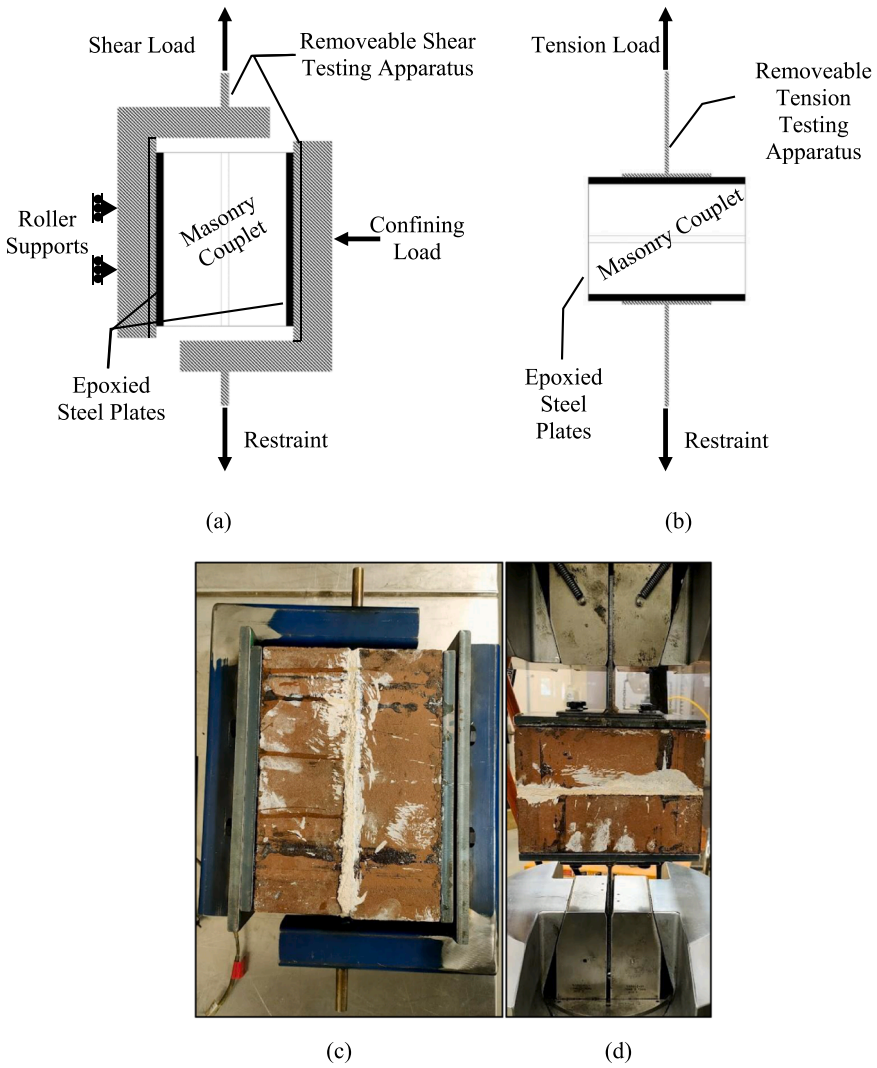

Fig. 2. Pilot study experimental testing arrangements. Schematic (a) shear testing and (b) tension testing apparatuses, and as-built (c) shear testing (not in universal testing machine, UTM), and (d) tension testing apparatuses.

epoxy for a minimum of 24-hours (and up to 72-hours to maximise the strength gain), significantly reduced the efficiency of testing. In addition to these issues, the shear testing method maintained a number of limitations. Firstly, the use of roller supports that were rigidly attached an external support, allowing for the relative movement of one of the masonry units (refer to Fig. 2(a) and (c)), introduced an additional, uncontrolled friction surface into the system between the shear-testing apparatus and the rollers. While these rollers were cleaned and greased, the high pre-compressions applied (up to 25.3 kN) required that large rollers be used to effectively transfer this load without significant deformations, thus increasing the friction losses into this support. Furthermore, as all specimens in this pilot stage of the study were pre-cracked prior to installation in the shear-testing apparatus, insertion of the couplet into the UTM for testing required care to minimise damage to the formed failure surface. This additional consideration significantly increased the difficulty associated with testing, as rotating the specimen parallel to the line of action of the UTM (refer to Fig. 2) encouraged the couplet to separate under self-weight.

2.3. Final test set-up

In addition to the pilot study discussed previously, there have been many studies that consider different methods of assessing the shear strength of the mortar bed joints. The study by Stöckl et al. [13] outlines six test methods and their performance in terms of normal and shear stress distributions, number of shear planes, the influence of perpend (head) joints and the difficulty of performing the test. Similarly, the experimental comparison of triplet and couplets testing setups performed by Segura et al. [15] noting that couplet tests produced notably higher shear strengths than triplet tests, a result that is attributable both to the distribution of stresses and the fact that a triplet test introduces additional uncertainty as two potential shear failure planes are introduced, such that the weaker of the two shear planes will always fail first. The current study does not utilise a shear triplet test method, such as is standardised in EN 1052–3 [11], due to the limitations noted in the literature, as well as a number of other key limitations. Firstly, the introduction of an additional shear plane makes the friction acting on a given mortar bed joint impossible to directly measure; rather an average of two frictional resistances would be determined. Additionally, the triplet test as specified in EN 1052–3 [11] is unsuitable for the measurement of the residual friction coefficient as once one of the two joints in a triplet cracks, the specimen tends to rotate, making the measurements of critical state behaviour unreliable. These limitations, and others, associated with the EN 1052–3 [11] triplet test are also noted in numerous previous studies, such as by Lawrence [16], Segura et al. [15] and Miccoli et al. [17].

To address these limitations, and those observed from the pilot study, the testing apparatuses shown in Fig. 3 were developed. For the shear

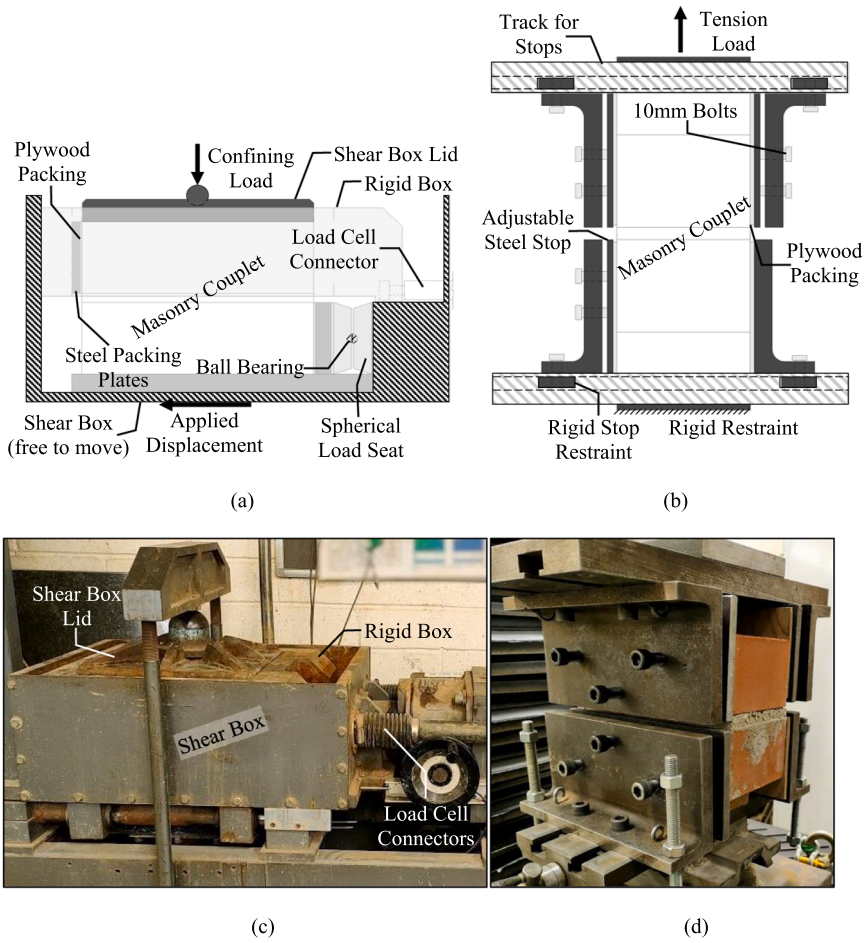

Fig. 3. Final experimental testing arrangements. Schematic (a) shear testing and (b) tension testing apparatuses, and as-built (c) shear testing and (c) tension testing apparatuses.

tests, a concept similar to that presented by Stöckl and Hofmann [18] was developed for fully bedded masonry couplets, via the application of a shear-box (as is commonly utilised in geotechnical testing), see Fig. 3 **(a)**. Pre-compression was applied to the specimen via a digitally force-controlled hydraulic jack, and shear forces were induced by applying a constant displacement to the shear box at a rate of 1.14 mm/min (refer to Fig. 3(a) and (c)). A vertically aligned spherical seat was installed on the bottom unit to ensure that full contact to the unit head was maintained throughout testing, and to compensate for any misalignment in the longitudinal axes of the units that may be evident as a result of poor workmanship. While the resultant testing apparatus introduced a non-uniform normal stress distribution along the mortar due to the offset between the lateral load restraints on the units, it is noted by Stöckl et al. [13] that this form of testing performs well by all other examined performance metrics (shear stress distribution, average normal stress, and number of shear planes and head joints).

For the tension tests, the laboratory study by Gooch et al. [19] was considered and improved upon. Specimens were gripped through the use of an adjustable steel plate with plywood packing (see Fig. 3(b) and (d)). Rigid steel stops were positioned on tracks to ensure that the application of load was concentric with the centre of the couplet before being locked in place. These stops maintained a secondary plate that could be extended and articulated in three-dimensions via three horizontal bolts. This allowed for a sufficiently high compressive force to be applied to restrain the specimens, via friction between the plywood and sides of the bricks, during testing.

While the consideration of a cracked section facilitates an investigation of the effect pre-existing damage has on the friction behaviour of masonry, the determination of a statistical description of the friction coefficient of clay-brick masonry is of key interest and was determined from testing of uncracked specimens. This was achieved by applying the developed shear testing method (refer to Fig. 3(a) and (c)) directly to uncracked specimens and recording the residual shear resistance and applied normal force.

3. Residual friction behaviour

3.1. Interpretation of data

A residual friction coefficient for each specimen was determined by considering the recorded load-displacement response. The uncracked specimens, as well as several of the cracked specimens, exhibited a peak shear resistance, followed by a residual shear capacity. Therefore, to characterise the residual friction coefficient, an average value was estimated from the load-displacement data in the critical state (residual) region. An example of this is presented in Fig. 4.

Furthermore, as shown in Fig. 1, all specimens, except for S1, maintained an interlocking mechanism: either mortar plugs (filled perforations for extruded units) or a frog (pressed units). These restraints against sliding influenced the behaviour of each couplet under direct shear loading. However, for all of the specimens tested in the current study, these interlocking mechanisms failed prior to the critical state, and as such, their influence on the residual frictional resistance is expected to be minimal.

Once the relevant mean residual shear resistance was determined, a residual friction coefficient was determined by the ratio of the mean

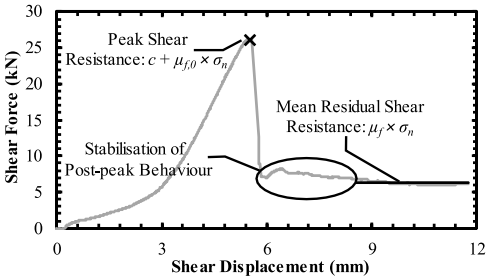

Fig. 4. Example of analysis of load-displacement behaviour.

residual shear force and the mean normal force acting over the same range. This value is equivalent to the ratio of the incremental shear forces over normal forces (recorded at a 0.5 s increments). Furthermore, in general, the variations in the normal forces in the post-peak region were minimal – see Table 1. A key observation was that the residual shear friction coefficient was highly dependent upon the normal stress, as shown in Fig. 5. Here, the mean residual friction coefficient at the minimum applied normal stress was 39 % to 83 % larger than at the maximum normal stress for the extruded units, and was 18 % to 29 % larger for the pressed/solid units. This behaviour is discussed in more detail in Section 3.2. As a result, residual friction coefficients have been pooled based both on the unit type and the nominal gross normal stresses (i.e.: 0.2 MPa, 0.6 MPa and 1.0 MPa) for the determination of the COVs shown in Table 1. Based on these subsets, it was observed that the COV of the residual friction coefficients ranged from 0.05 to 0.18, comparable to the COV of clay-brick masonry's compression strength – commonly considered to be between 0.10 to 0.15 [4,20,21].

This restriction to the pooling of data based on the applied normal force significantly increases the number of specimens required to accurately define a probabilistic model of the friction coefficient. However, the three examined extruded unit types exhibited similar behaviour and dependence on the applied normal stress. Similarly, the responses of the two pressed unit and single solid unit types were similar. As such, a probabilistic model of μ_f can be reasonably determined by pooling the data of E1, E2 and E3, and of P1, P2 and S1 into two distinct subsets.

3.2. Normal stress dependence

The normal stress dependence of the residual friction coefficient observed during testing is significant, particularly across the range of

Table 1
Results of uncracked couplet shear tests.

Specimen Type	Sample Size	Mean Normal Stress, σ_n (MPa)	Mean Residual Friction Coefficient, μ_f
	10	0.22 [0.06]	1.10 [0.18]
E1	10	0.60 [< 0.01]	0.82 [0.07]
	10	1.00 [< 0.01]	0.60 [0.10]
	10	0.21 [0.05]	1.11 [0.09]
E2	10	0.60 [< 0.01]	0.96 [0.07]
	10	1.00 [< 0.01]	0.80 [0.06]
	10	0.21 [0.04]	1.11 [0.09]
E3	10	0.60 [< 0.01]	0.95 [0.05]
	10	1.00 [< 0.01]	0.81 [0.12]
	10	0.22 [0.08]	1.04 [0.15]
P1	10	0.60 [< 0.01]	0.94 [0.12]
	10	1.00 [< 0.01]	0.88 [0.09]
	10	0.22 [0.08]	1.16 [0.16]
P2	10	0.60 [< 0.01]	0.99 [0.10]
	10	1.00 [< 0.01]	0.91 [0.12]
	10	0.21 [0.08]	1.06 [0.14]
S1	10	0.60 [< 0.01]	0.91 [0.12]
	10	1.00 [< 0.01]	0.82 [0.10]

Note: COVs are shown in [].

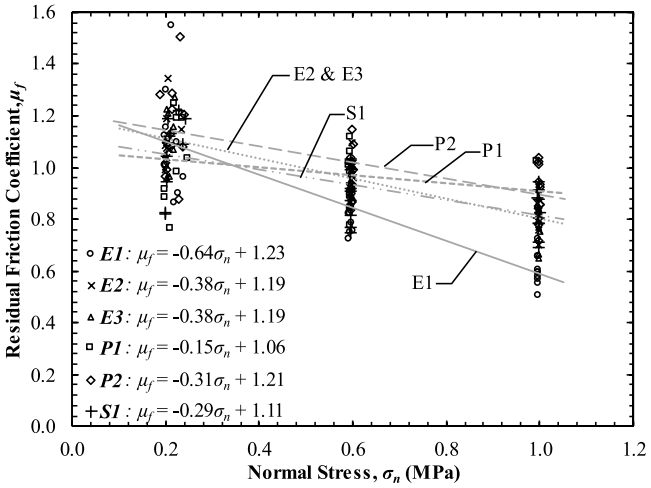

Fig. 5. Friction coefficient, μ_f, versus applied gross normal stress, σ_n.

pre-compressive stresses that are common in non-residential load-bearing masonry walls. This dependence may be attributable to the influence of dilatancy on the observed shearing angle, ϕ', where $\tan(\phi') = \mu_f$. This area of research is well established in the field of soil mechanics. Bolton [22] presents a saw blades model of dilatancy that highlights this behaviour, as shown in Fig. 6. Here, ϕ_{crit}' is the shearing angle of a loose soil, or one that is in its critical (post-peak) state, with no dilation. If this same soil is tested dense, and in a pre-critical state, shearing must either overcome points of contact between particles or crush the particles. Assuming that particles above the zero-extension line Z-Z (refer to Fig. 6) form a rigid zone sliding upwards at an angle of ψ over the rigid zone beneath, shearing occurs along an inclined microfacet (S-S) upon which there is no dilation, and the angle of shearing remains at ϕ_{crit}'. The observed shear angle, ϕ', is then the sum of the critical state friction angle, ϕ_{crit}', and the angle of the inclined shear plane, S-S, to the zero-extension line, denoted as the dilatancy angle, ψ [22].

A limitation of Bolton's model in the context of masonry unit-mortar interface sliding is that dilatancy is not present in the critical state shear behaviour of soils due to the loosening of material via volumetric strain change. However, for rigid-body materials such as bricks and mortar, rock joints, concrete, etc., only the degradation of interface roughness (equivalent to the crushing of contacting particles) is possible. As such, the influence of dilatancy on the residual interface friction between rigid materials may be significant. Furthermore, the effective dilatancy angle is proportional to the amount of stress acting perpendicular to the plane of shearing for both soils [22] and unit-mortar interfaces [23]. Instances of greater normal stress will exhibit a smaller effective dilatancy angle (and, therefore, observed shearing angle) as the displacement required to overcome the contacting particles must act against any confining stress, and thus a greater degree of particle/surface roughness crushing will occur before the critical state is achieved.

In the current study, the relatively small normal force of 5.1 kN (equivalent to 0.2 MPa of gross normal stress) would be expected to

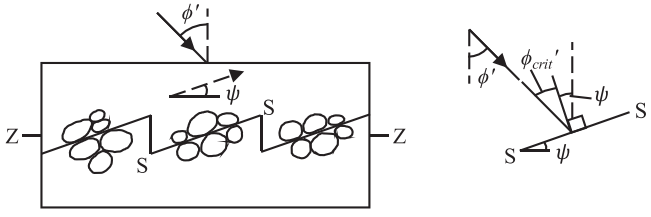

Fig. 6. The saw blades model of dilatancy. (adapted from [22]).

produce a relatively rough critical shear surface, with a correspondingly high observed friction coefficient. However, as the normal forces considered in this study were increased to 15.1 kN and to 25.3 kN (0.6 MPa and 1.0 MPa equivalent gross normal stresses), the opposing sliding planes would be further restrained against vertical displacement, resulting in additional crushing, reducing the dilatancy angle and smoothing the critical state shear failure surface such that a lower observed shearing angle (and, therefore, lower residual friction coefficient) would be observed (see Fig. 7). Furthermore, considering the live-to-dead load ratios and typical tributary areas for structural elements outlined by Ellingwood et al. [24] and Pham [25], compressive stresses ranging between 0.2 MPa and 1.0 MPa represent a typical range of loads that URM shear walls would be subject to at the ultimate limit state.

As a result of the influence of dilatancy and the subsequent dependence of shear angle upon the applied normal stress, a predictive model of the normal stress dependence of μ_f was developed by performing additional testing on each specimen type at the gross normal stresses of 2.0 MPa and 3.0 MPa. The results of these twelve additional tests, as well as the mean residual friction coefficients at each of the examined gross normal stress levels, indicates that an exponential function produced the best fit to the data. The derived predictive models of the residual friction coefficient as a function of normal stress, $\mu_{f,pred}$, are shown in Fig. 8.

3.3. Probability models of the residual friction coefficient

Due to the dependence of the residual friction coefficient on the normal stress, a suitable proxy for pooling the data across each subset of normal stress was required to define μ_f in probabilistic terms. For this, the model error (*ME*) of the predictive models shown in Fig. 8 was used – where, $ME = \mu_{f,test} / \mu_{f,pred}$. The derived functions of residual friction coefficient, $\mu_{f,pred}$, were developed such that the sample means of *ME* for both the extruded and pressed/solid subsets were equal to 1.0 (equivalent to a perfect representation). Furthermore, from these pooled datasets, the COV of *ME* for both masonry subsets was found to equal 0.14.

From the data presented in Fig. 5, totals of 90 values of $\mu_{f,test} / \mu_{f,pred}$ were determined both for the extruded and the pressed/solid masonry couplets. A number of probability distributions were then fitted to these values using the method of maximum likelihood for the parameter estimation. These distributions were the Normal (Gaussian), Lognormal, Gamma, Gumbel (extreme value type I), and Weibull (extreme value type III). The fitted probability density functions (PDFs) are presented in Fig. 9(a) and (c). To determine the most suitable of these models, the Kolmogorov-Smirnov (K-S) and Anderson-Darling (A-D) tests were performed; however, only the Gumbel distribution fitted to the data for the pressed/solid units was rejected at the 5 % significance level. Therefore, a suitable probabilistic model was determined via a qualitative best-fit examination of the inverse cumulative distribution functions (CDF^{-1}) versus the determined values of *ME* – see Fig. 9(b) and (d). Here, it may be seen that the Normal distribution with mean = 1.0 and COV = 0.14 produces the best overall fit to the data, particularly in the lower tails; the portion of the model that most significantly affects structural reliability.

The experimentally measured variability ($COV_{measured}$, equivalent to COV_{ME}) for both test specimens includes the variability of μ_f, as well as the variability introduced into the laboratory testing due to inaccuracies in the gauges, read outs and definitions values (COV_{test}), and the variability caused by differences between the strengths or geometries of the experimental specimens relative to a control specimen (COV_{spec}) [24]. As such, the variability of μ_f is determined as:

$$COV_{\mu_f} = \sqrt{COV_{ME}^2 - COV_{test}^2 - COV_{spec}^2} \quad (1)$$

The study by Gooch et al. [26] found that a value of $COV_{spec} = 0.01$ was reasonable for full-scale masonry shear walls. As the specimens utilised in the current study are a single unit in length and width, the value of COV_{spec} is largely subject to the manufacturing tolerances of clay-brick masonry unit which has been found to maintain a COV < 0.01. The main source of test variability was in the variability of the normal stress in the critical state region, particularly for the 0.2 MPa nominal normal stress specimens. As the variability of the normal stresses was distinct for each nominal normal stress level, COV_{test} has been determined by a Monte-Carlo simulation, using the experimental means and COVs shown in Table 1 and assuming a Normal distribution of normal stresses. From this analysis, a value of $COV_{test} = 0.05$ was determined.

Considering the determined values of $COV_{measured}$, COV_{test} and COV_{spec}, as well as the mean *ME* equal to 1.0 and the predictive equations shown in Fig. 8, the probabilistic models of μ_f shown in Table 2 have been derived.

4. Influence of tension-cracked Joints

The second phase of the testing program consisted of similar direct shear testing to that discussed in previous sections, performed on masonry couplets that were pre-cracked under direct tension loading. Magenes and Calvi [2] suggest that the friction coefficient for tension-cracked mortar joints should be greater than the residual friction coefficient of a sliding mortar joint. This behaviour may be expected as the failure surface formed under direct tensile loading has not been subjected to surface roughness degradation resulting from shearing (refer to Section 3.2). To assess the influence of tension cracking on the friction resistance of masonry, three additional direct shear tests were performed per nominal gross normal stress (0.2 MPa, 0.6 MPa, and 1.0 MPa) and per specimen type, for a total of 54 additional specimens. These specimens were first subject to direct tension loading as discussed in Sections 2.2 and 2.3, prior to shearing under a constant applied normal force.

For the extruded masonry specimens, the mean cracked residual friction coefficient, $\mu_{f,cr}$, ranged from 0.53 at 1.0 MPa to 1.34 at 0.2 MPa (see Table 3), compared to the range of mean coefficients between 0.60 and 1.11 for the uncracked specimens. This difference constitutes an average ratio of $\mu_{f,cr} / \mu_f = 0.94$. However, there was disagreement between the results of the different extruded masonry types. For E1 and E2, average ratios of $\mu_{f,cr} / \mu_f = 0.86$ and 0.84 were observed, respectively, while E3 exhibited a mean value of $\mu_{f,cr} / \mu_f = 1.08$. Furthermore, while the friction resistance of the E1 and E2 specimens was, on average, reduced as a result of pre-induced tension cracking, this reduction is minor and may not necessarily be attributable to the induced cracking

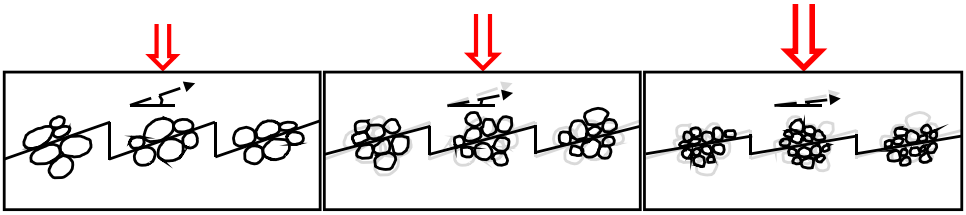

Fig. 7. Influence of confinement on dilatancy and shearing angles.

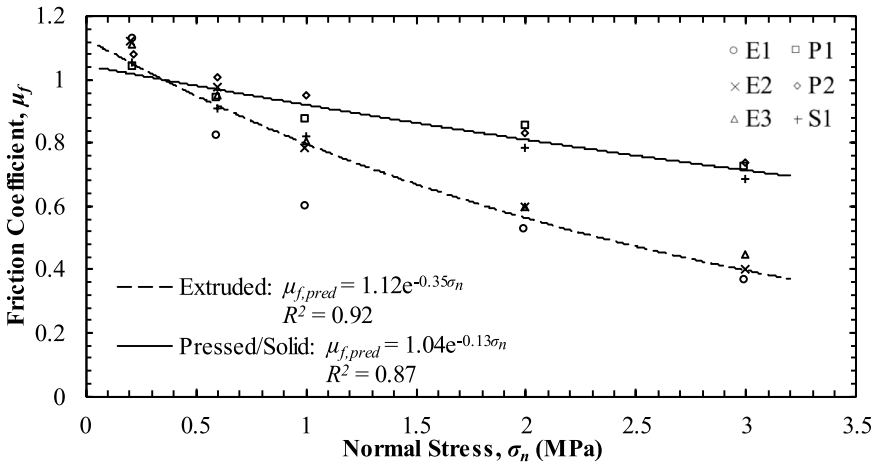

Fig. 8. Predictive models of residual friction coefficient as a function of gross normal stress.

due to the inherent variability of the friction coefficient, as well as the greater possibility of disturbing the critical state failure surface as specimens are transferred from the tension testing apparatus to the shear box. Similar observations were made for the pressed and solid masonry specimens, where $\mu_{f,cr}$, ranged from 0.80 at 1.0 MPa to 1.38 at 0.2 MPa, compared to the range of uncracked means of 0.82 to 1.16. There was a greater degree of consistency between the overall averages of $\mu_{f,cr} / \mu_f$ with values of 1.03, 1.08 and 1.10 for P1, P2 and S1, respectively. Finally, considering all specimens in aggregate, an overall mean value of $\mu_{f,cr} / \mu_f = 1.01$ was determined. These results indicate that the presence of tension cracks does not significantly affect the residual friction coefficient of masonry joints. It should be noted that, due to the relatively few cracked specimens examined in this study (three specimens per unique specimen type and pre-compression), additional testing of cracked couplets may provide a more accurate estimate of $\mu_{f,cr} / \mu_f$.

5. Relationship to the initial friction coefficient

Unlike the residual friction coefficients that have been discussed thus far, the initial friction coefficient, $\mu_{f,0}$, cannot be readily determined for an individual test specimen. This is because the initial frictional resistance occurs at the peak shear resistance, which is the combination of the frictional resistance and the shear bond strength (cohesion) (see Fig. 4). While the shear bond strength of masonry can be reasonably determined from direct shear tests on unconfined masonry ($\sigma_n = 0$), the initial frictional resistance cannot be as easily isolated from the shear bond strength. Instead, a common method of estimating both the shear bond strength and initial friction coefficient is to undertake a series of confined shear tests under differing levels of normal stress, and then to perform a linear regression analysis of the peak shear stress versus normal stress to determine a y-axis intercept (shear bond strength) and line slope (friction coefficient). EN 1052–3 [11] specifies that at least nine specimens, three at each gross nominal normal stress of 0.2 MPa, 0.6 MPa and 1.0 MPa, must be tested. While EN 1052–3 [11] specifies a triplet test, rather than the couplet tests performed in the current study, the peak shear resistance of each specimen is readily determinable from the collected data.

Considering the thirty specimens of each masonry type (ten at each nominal pre-compression), the peak shear stresses and subsequent linear regression analysis results are presented in Fig. 10. It is notable in Fig. 10 that a number of specimens – particularly those tested at the lower 0.2 MPa nominal normal stress – maintain a measured normal stress significantly higher than the target stress, despite the use of a digital force controller that increased or decreased the hydraulic pressure to maintain the target normal stress. This is a result of two factors. Firstly, due to the tendency of the specimens to dilate under shear loading (see discussion in Section 3.2), additional normal stress is introduced onto the mortar joint (and into the vertically aligned load cell) as the top brick in each couplet attempts to displace vertically. This behaviour is evident in the results presented in Fig. 5 and Tables 1 and 3, though it is more prominent in the results shown in Fig. 10 as only a single data point is considered, and so the sensitivity to error is far greater. Secondly, the vertically aligned hydraulic jack used the in tests maintained a 100 kN capacity. This capacity was useful in the current study as it allowed specimens to be tested at (and above) a 3 MPa nominal gross normal stress. However, for specimens tested at low pre-compression (such as the 5.1 kN nominal force corresponding to a 0.2 MPa normal stress), the hydraulic jack was unable to efficiently adjust the normal force to align with the target. This limitation is evident in the greater consistency in normal stress seen in the 0.6 MPa and 1.0 MPa specimens. It should however be noted that, as with the determination of the residual friction coefficient, all test results for the peak shear resistance consider the measured normal force (or equivalent gross normal stress), rather than the nominal target stress.

The determined shear bond strengths, ranging from 0.58 MPa to 1.04 MPa are consistent with the literature, as are the initial friction coefficients determined via linear regression analysis between 0.64 and 1.00 [27-30]. However, in comparison to the residual cracked and uncracked friction coefficients determined in the current study, the initial friction coefficients shown in Fig. 10 are notably low. It is reasonable to expect that the initial friction coefficient would be greater than (or equal to) the residual friction coefficient as it corresponds to the frictional resistance of a failure surface that has not been degraded via surface roughness degradation (refer to Section 3.2). However, considering the exponential models derived in Section 3.2, the determined values of $\mu_{f,0}$ correspond to a heavily confined frictional interface ($\sigma_n = 1.5$ MPa, considering the six specimen types in aggregate). Furthermore, the overall mean value of $\mu_{f,0} / \mu_f = 0.91$ indicates that, on average, the determined initial friction resistance is lower than the residual friction resistance. It should be noted, however, that the coefficients of determination (R^2) are low (refer to Fig. 10), indicating that the linear regression models do not capture the high variability in the observed peak shear stress values. While this result is not unexpected; the values of τ_p in Fig. 10 consider the variabilities in the test, specimens and materials (shear bond and friction), it indicates that there is significant uncertainty associated with the friction coefficients derived in this manner. To capture this, the 95th percentile confidence limits of $\mu_{f,0}$ are shown in Table 4.

The comparison between the initial, $\mu_{f,0}$, and cracked, $\mu_{f,cr}$, friction coefficients is also significant. Although the bond strength of the cracked specimens is destroyed prior to shearing, no degradation of the interface roughness should be present during the second-stage shear testing. In

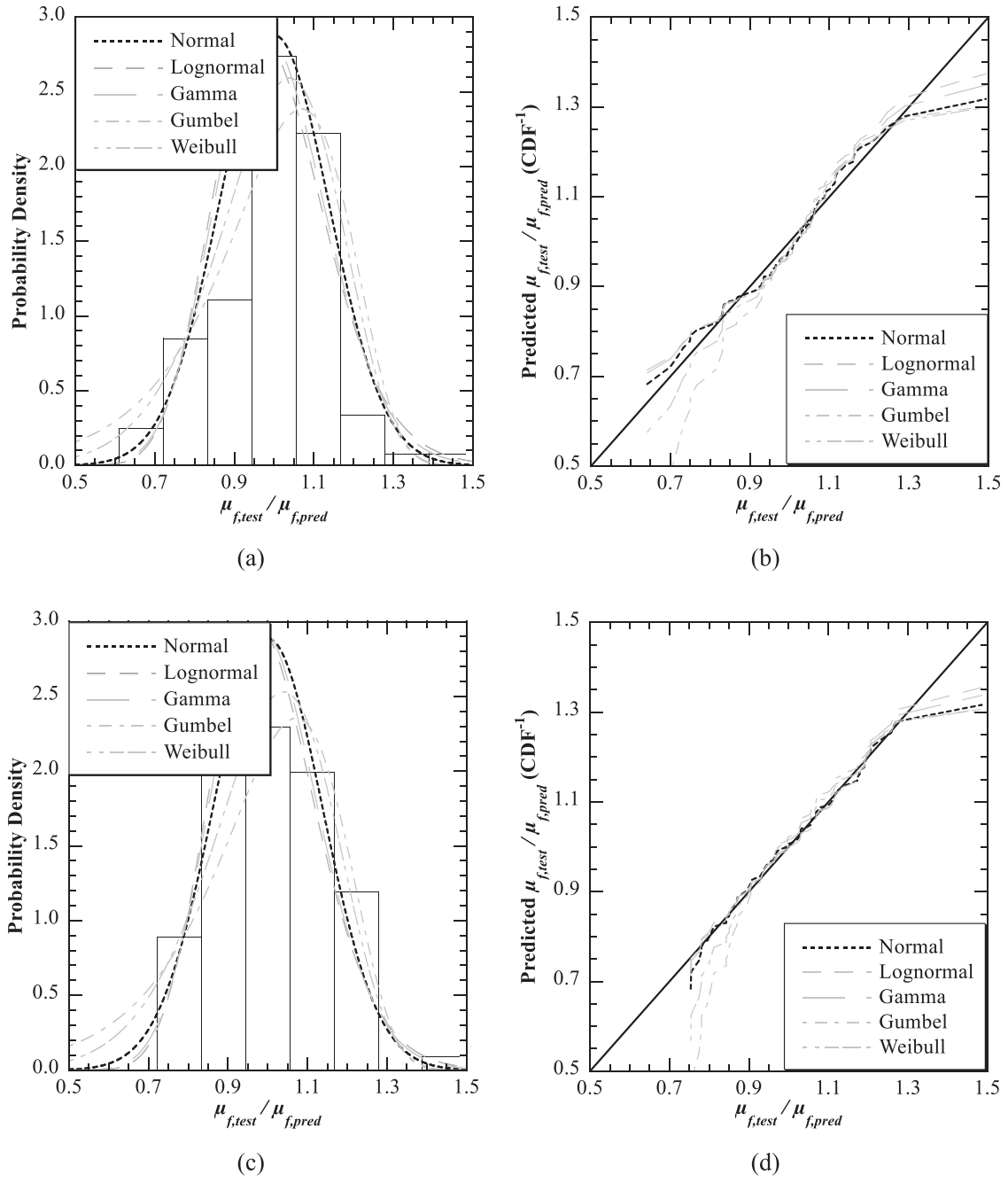

Fig. 9. Fitted (a) PDFs and (b) CDF^{-1} of $\mu_{f,test}$ / $\mu_{f,pred}$ for extruded masonry couplets, and (c) PDFs and (d) CDF^{-1} of $\mu_{f,test}$ / $\mu_{f,pred}$ for pressed/solid masonry couplets.

Table 2
Probabilistic description of the residual friction coefficient, μ_f, of clay-brick masonry.

Parameter	Masonry Type	
	Extruded	Pressed/Solid
Mean	$1.12 \bullet e^{-0.35 \bullet \sigma n}$	$1.04 \bullet e^{-0.13 \bullet \sigma n}$
COV	0.13	
Distribution	Normal	

reality, there was certainly a degree of disturbance to the developed failure surface despite efforts to prevent this. Furthermore, factors prior to the establishment of a stable shear resistance such as the initial application of normal force, the closure of gaps, compression of packing plywood, etc. would act to degrade the interface roughness. However, it is reasonable to expect that the friction coefficients determined of these interfaces would more closely align with the estimates of the initial friction coefficient. The comparisons between $\mu_{f,0}$ / $\mu_{f,cr}$ shown in Table 4, however, are largely consistent with those for $\mu_{f,0}$ / μ_f.

The inconsistency between the directly measured residual friction coefficients and the initial friction coefficient determined via linear regression is significant as it may highlight a limitation of the method outlined in EN 1052–3 [11], perhaps the most common technique for estimating the frictional resistance of masonry. Considering the saw blades model of dilatancy by Bolton [22], the initial angle of shearing is the sum of the critical state (residual) shearing angle and the dilatancy angle (refer to Fig. 6). For dense soils, the effective dilatancy is destroyed in the critical state by the loosening of material and the crushing of soil particles, resulting in an angle of shearing equal to the critical state shearing angle. While rigid materials such as masonry are not subject to

Table 3
Results of direct tension and cracked couplet shear tests.

Specimen Type	Direct Tension Bond Strength, f_t (MPa)	Testing Method[1]	Sample Size	Normal Stress, σ_n, (MPa)	Mean Cracked Residual Friction Coefficient, $\mu_{f,cr}$	$\mu_{f,cr}$ / μ_f
			3	0.20 [< 0.01]	0.97 [0.21]	0.88
E1	0.17 [0.42]	*Pilot*	3	0.60 [0.01]	0.66 [0.12]	0.80
			3	1.00 [< 0.01]	0.53 [0.17]	0.88
			3	0.20 [< 0.01]	1.11 [0.30]	1.00
E2	0.21 [0.22]	*Pilot*	3	0.60 [< 0.01]	0.77 [0.17]	0.80
			3	1.00 [< 0.01]	0.58 [0.32]	0.73
			3	0.22 [< 0.01]	1.34 [0.02]	1.21
E3	0.25 [0.18]	*Final*	3	0.60 [< 0.01]	1.08 [0.08]	1.14
			3	1.00 [< 0.01]	0.86 [0.13]	1.06
			3	0.22 [0.05]	1.08 [0.24]	1.04
P1	0.15 [0.59]	*Final*	3	0.60 [0.01]	0.98 [0.15]	1.04
			3	1.00 [< 0.01]	0.89 [0.03]	1.01
			3	0.22 [< 0.01]	1.38 [0.02]	1.19
P2	0.25 [0.18]	*Final*	3	0.60 [< 0.01]	1.08 [0.08]	1.09
			3	1.00 [< 0.01]	0.86 [0.13]	0.95
			3	0.24 [< 0.01]	1.32 [0.01]	1.25
S1	0.22 [0.20]	*Final*	3	0.60 [< 0.01]	0.97 [0.03]	1.07
			3	1.00 [< 0.01]	0.80 [0.08]	0.98
					Overall Mean:	**1.01**

Note: COVs are shown in [].
1 Refer to Section 2.

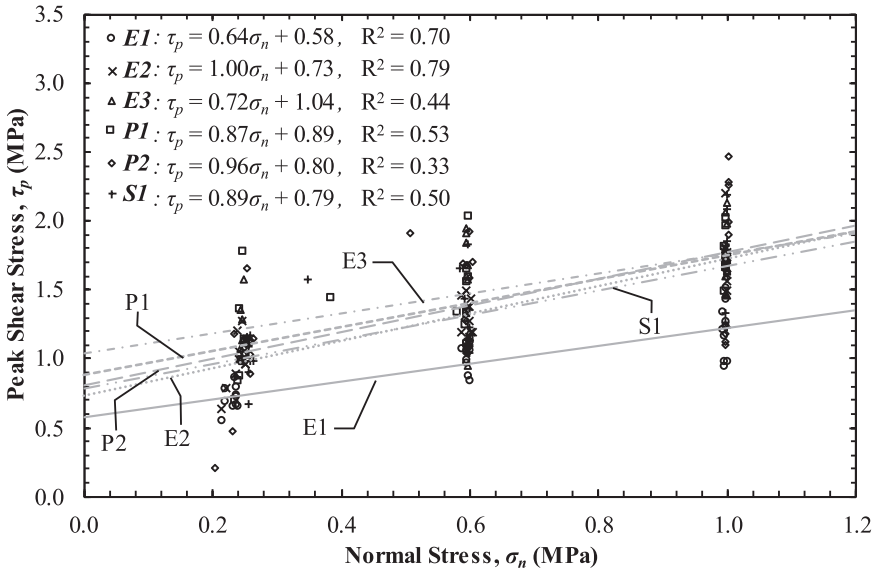

Fig. 10. Peak gross shear stress, τ_p, versus gross normal stress, σ_n.

a significant volumetric strain change, degradation of the effective dilatancy is still expected – particularly under higher levels of confinement – and thus the residual friction coefficient should be no greater than the initial friction coefficient. The inconsistency of the determined initial friction coefficients with this well-established model, as well as the fact that a linear regression analysis does not consider the expected normal stress dependence, likely results in the friction coefficient being underrepresented at lower normal stresses and overrepresented at higher normal stresses.

However, while the initial friction coefficients determined in Fig. 10 may not be representative of the true friction resistance, the values are conservative for the level of pre-compressive stress expected in typical URM structures. Additionally, in most numerical models for URM sliding behaviour, dilatancy is considered via the definition of an initial and residual friction angle, and a dilatancy angle.

6. Conclusions

An experimental study was conducted to produce a probabilistic characterisation of the residual friction coefficient of the masonry unit-mortar interface. It was found that for extruded (perforated), pressed (frogged) and solid masonry types, the residual friction coefficient is dependent upon the normal stress acting on the shear plane. To account for this dependence, direct shear tests were performed on masonry couplets under nominal gross normal stresses between 0.2 MPa and 3.0 MPa. The results of these tests indicated that an exponential predictive model most accurately represented the relationship between residual friction coefficient and normal stress. Utilising this predictive model, it was determined that a Normal (Gaussian) distribution produced a reasonable representation of the experimental data, with a mean value determined in accordance with the derived predictive models and a coefficient of variation equal to 0.14. Furthermore, nine additional direct shear tests per masonry type (three each at nominal gross normal stresses of 0.2 MPa, 0.6 MPa and 1.0 MPa) were performed on

Table 4
Comparison of initial friction coefficient, $\mu_{f,0}$, determined via linear regression analysis to uncracked, μ_f, and cracked, $\mu_{f,cr}$, residual friction coefficients.

Specimen Type	$\sigma_{n,nominal}$ (MPa)	μ_f	$\mu_{f,0}$	$\mu_{f,0}$ / μ_f	$\mu_{f,cr}$	$\mu_{f,0}$ / $\mu_{f,cr}$
E1	0.20	1.10	0.64 ± 0.16	0.59	0.97	0.66
	0.60	0.82		0.79	0.66	0.98
	1.00	0.60		1.07	0.53	1.22
E2	0.20	1.11	1.00 ± 0.20	0.89	1.11	0.89
	0.60	0.96		1.03	0.77	1.28
	1.00	0.80		1.24	0.58	1.70
E3	0.20	1.11	0.72 ± 0.31	0.65	1.34	0.54
	0.60	0.95		0.76	1.08	0.67
	1.00	0.81		0.89	0.86	0.84
P1	0.20	1.04	0.87 ± 0.31	0.83	1.08	0.80
	0.60	0.94		0.92	0.98	0.88
	1.00	0.88		0.98	0.89	0.97
P2	0.20	1.16	0.96 ± 0.54	0.83	1.38	0.70
	0.60	0.99		0.97	1.08	0.89
	1.00	0.91		1.06	0.86	1.12
S1	0.20	1.06	0.89 ± 0.34	0.84	1.32	0.67
	0.60	0.91		0.98	0.97	0.92
	1.00	0.82		1.08	0.80	1.11
Overall Mean:				0.91		0.94

specimens that were first cracked under direct tension loading. The mean ratios between pre-cracked and uncracked friction coefficients ranged from 0.84 to 1.10, with an overall mean ratio of 1.01. These results indicate that the presence of existing tension cracks has minimal influence on the effective friction coefficient of mortar joints. Finally, considering the peak shear resistance of each uncracked masonry couplet, the initial friction coefficient was determined via a linear regression analysis in accordance with EN 1052–3 [11]. These results indicate that initial friction coefficients determined in this manner are notably inaccurate, though conservative, due to a lack of accounting for the normal stress dependence of the angle of shearing.

CRediT authorship contribution statement

Michele Spadari: Resources, Methodology, Investigation. **Mark G. Stewart:** Writing – review & editing, Validation, Supervision, Project administration, Funding acquisition, Conceptualization. **Mark J. Masia:** Writing – review & editing, Validation, Supervision, Project administration, Funding acquisition, Conceptualization. **Lewis J. Gooch:** Writing – review & editing, Writing – original draft, Visualization, Validation, Methodology, Investigation, Formal analysis, Data curation, Conceptualization.

Declaration of Competing Interest

The authors declare the following financial interests/personal relationships which may be considered as potential competing interests: Mark J. Masia reports financial support was provided by Australian Research Council. Mark G. Stewart reports financial support was provided by Australian Research Council. If there are other authors, they declare that they have no known competing financial interests or personal relationships that could have appeared to influence the work reported in this paper.

Acknowledgements

This research was funded by the Australian Research Council under Discovery Project DP220102758. The authors gratefully acknowledge the contributions of The University of Newcastle's laboratory technical staff. The support provided by Think Brick Australia in providing brick units is gratefully recognised.

Data Availability

Data will be made available on request.

References

[1] Turnšek, V. & Čačovič, F. Some experimental results on the strength of brick masonry walls. Proceedings of the 2nd International Brick Masonry Conference, Stoke-on-Trent, 1970.
[2] G. Magenes, G.M. Calvi, In-plane seismic response of brick masonry walls, Earthq. Eng. Struct. Dyn. 26 (1997) 1091–1112, https://doi.org/10.1002/(SICI)1096-9845(199711)26:11<1091::AID-EQE693>3.0.CO;2-6.
[3] NTC, Decreto del ministero delle infrastrutture, supplemento ordinario n.8 alla gazzetta ufficiale n. 42 della Repubblica Italiana, Norme Tecniche per le Costruzioni, Rome, 2018.
[4] SAI, AS3700: Masonry Structures, Standards Australia, Sydney, 2018.
[5] CEN, EN1996-1-1: Eurocode 6: Design of masonry structures - Part 1-1: General rules for reinforced and. Unreinforced masonry structures, European Committee for Standardization, Brussels, 2022.
[6] TMS, TMS 402/602-22 Building Code Requirements and Specification for Masonry Structures, The Masonry Society, Colorado, 2022.
[7] CSA, S304-24: Design of Masonry Structures, Canadian Standards Association, Mississauga, 2024.
[8] T. Manzouri, M.P. Schuller, P.B. Shing, B. Amadei, Repair and retrofit of unreinforced masonry structures, Earthq. Spectra 12 (1996) 903–922, https://doi.org/10.1193/1.1585916.
[9] M.J. Masia, R.B. Petersen, Y. Han, M.R.S. Corrêa, Torsion shear test for mortar joints in masonry: experimental, Eval. Mason. Int. 23 (2010) 91–102.
[10] A.H. Salmanpour, N. Mojsilović, J. Schwartz, Displacement capacity of contemporary unreinforced masonry walls: an experimental study, Eng. Struct. 89 (2015) 1–16, https://doi.org/10.1016/j.engstruct.2015.01.052.
[11] CEN. EN1052-3: Methods of test for masonry. Part 3: Determination of initial shear strength. Brussels: European committee of standardization, 2002.
[12] S. Gonen, B. Pulasu, E. Erdogmus, P.B. Lourenço, S. Soyoz, Effects of spatial variability and correlation in stochastic discontinuum analysis of unreinforced masonry walls, Constr. Build. Mater. 337 (2022), https://doi.org/10.1016/j.conbuildmat.2022.127511.
[13] S. Stöckl, P. Hofmann, J. Mainz, A comparative finite element evaluation of mortar joint shear tests, Mason. Int. 3 (1990) 101–104.
[14] R. Van Der Pluijm. Material properties of masonry and its components under tension and shear. Proceedings of the 6th Canadian Masonry Symposium, Saskatoon, 1992.
[15] J. Segura, E. Bernat, V. Mendizábal, L. Pelà, P. Roca, L. Gil, Experimental comparison of two testing setups for characterizing the shear mechanical properties of masonry, J. Build. Eng. 44 (2021), https://doi.org/10.1016/j.jobe.2021.103277.
[16] Lawrence, S.J.. Behaviour of brick masonry walls under lateral loading. Ph.D., University of New South Wales, 1983.
[17] L. Miccoli, D. Ferretti, E. Michelini, F. Loderer, Determination of the initial shear strength of AAC masonry with and without pre-compression according to EN1052-3. Proceedings of the 7th International Conference on Autoclaved Aerated Concrete, A Wiley Brand, Prague. Ernst & Sohn, 2023, pp. 191–197.
[18] S. Stöckl, P. Hofmann, Tests on the shear-bond behaviour in the bed-joints of masonry, Mason. Int. (1986) 9.
[19] L.J. Gooch, M.J. Masia, M.G. Stewart, C.Y. Lam, Statistical assessment of tensile and shear properties of unreinforced clay brick masonry, Constr. Build. Mater. 386 (2023), https://doi.org/10.1016/j.conbuildmat.2023.131578.
[20] Al-Harthy, A.S. & Frangopol, D.M. Reliability analysis of masonry walls. Proceedings of the 7th Specialty Conference on Probabilistic Mechanics and Structural Reliability, 1996 Worcester, MA. American Society of Civil Engineers, 338-341.
[21] M.G. Stewart, S.J. Lawrence, Model error, structural reliability and partial safety factors for structural masonry in compression, Mason. Int. 20 (2007) 107–116.
[22] M.D. Bolton, The strength and dilatancy of sands, Géotechnique 36 (1986) 65–78, https://doi.org/10.1680/geot.1986.36.1.65.
[23] P.B. Lourenço. Computational Strategies for Masonry Structures. Ph.D., Delft University of Technology, 1996.
[24] B.R. Ellingwood, T.V. Galambos, J.G. Macgregor, C.A. Cornell, Development of a Probability Based Load Criterion for American National Standard A58, National Bureau of Standards, Washington D.C., 1980.
[25] L. Pham, Load combinations and probabilistic load models for limit state codes, Civ. Eng. Trans. CE27 (1985) 62–67.
[26] L.J. Gooch, M.G. Stewart, M.J. Masia, Accuracy of stochastic finite element analyses for the safety assessment of unreinforced masonry shear walls, Civ. Eng. Environ. Syst. (2024) 1–30, https://doi.org/10.1080/10286608.2024.2400960.
[27] L.J. Gooch, M.J. Masia, M.G. Stewart, M.A. Hossain, Experimental testing of unreinforced masonry shear walls and comparison with nominal capacity predictions, J. Struct. Eng. 151 (2025), https://doi.org/10.1061/JSENDH.STENG-13877.

[28] Heffler, L.M.. Variability of Unit Flexural Bond Strength and its Effect on Strength in Clay Brick Unreinforced Masonry Walls Subject to Vertical Bending. MPhil, The University of Newcastle, Australia, 2009.

[29] G. Milani, P.B. Lourenço, Simple homogenized model for the nonlinear analysis of FRP-strengthened masonry structures. Part II: structural applications, J. Eng. Mech. 139 (2013) 77–93, https://doi.org/10.1061/(ASCE)EM.1943-7889.0000479.

[30] Lawrence, S.J.. Behaviour of brick masonry walls under lateral loading. Ph.D., University of New South Wales, 1983.